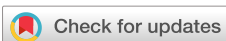


RESEARCH ARTICLE | DECEMBER 07 2020

Two-band whistler-mode waves excited by an electron bi-Maxwellian distribution plus parallel beams

Huayue Chen  ; Konrad Sauer  ; Quanming Lu  ; Xinliang Gao  ; Shaojie Wang 



AIP Advances 10, 125010 (2020)

<https://doi.org/10.1063/5.0026220>



View
Online



Export
Citation

Articles You May Be Interested In

Whistler waves with electron temperature anisotropy and non-Maxwellian distribution functions

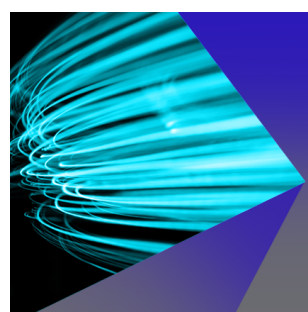
AIP Advances (May 2018)

2D particle-in-cell simulations of the electron temperature anisotropy driven whistler instability in plasmas having kappa velocity distributions

Phys. Plasmas (June 2021)

Formation of electron kappa distributions due to interactions with parallel propagating whistler waves

Phys. Plasmas (February 2014)



AIP Advances

Special Topics Now Online

[Learn More](#)

AIP Publishing

Two-band whistler-mode waves excited by an electron bi-Maxwellian distribution plus parallel beams

Cite as: AIP Advances 10, 125010 (2020); doi: 10.1063/5.0026220

Submitted: 14 October 2020 • Accepted: 17 November 2020 •

Published Online: 7 December 2020



View Online



Export Citation



CrossMark

Huayue Chen,^{1,2,a)} Konrad Sauer,^{3,a)} Quanming Lu,^{1,2} Xinliang Gao,^{1,2} and Shaojie Wang⁴

AFFILIATIONS

¹CAS Key Laboratory of Geoscience Environment, School of Earth and Space Sciences, University of Science and Technology of China, Hefei 230026, China

²CAS Center for Excellence in Comparative Planetology, Hefei 230026, China

³Max-Planck-Institute for Solar System Research, Göttingen 37077, Germany

⁴CAS Key Laboratory of Geoscience Environment, Department of Modern Physics, University of Science and Technology of China, Hefei 230026, China

^{a)}Authors to whom correspondence should be addressed: huayue_chen@foxmail.com and sauer.ka@gmail.com

ABSTRACT

The characteristics of whistler-mode waves excited by temperature anisotropic electrons, whose velocity distribution is a combination of bi-Maxwellian distribution and beam-like shapes, are investigated by both linear theory analysis and particle-in-cell simulation. A frequency gap is formed between two peaks, which is caused by the mode splitting of beam-like electrons. We have further investigated the influences of different parameters and found that the position of beam-like shape is the key parameter in determining the frequency of power gap. Moreover, the beam-like component on one direction will lead to the gap in the spectra of waves propagating in the opposite direction. Our study can shed light on the effects of beam-like electrons on the spectra of whistler-mode waves.

© 2020 Author(s). All article content, except where otherwise noted, is licensed under a Creative Commons Attribution (CC BY) license (<http://creativecommons.org/licenses/by/4.0/>). <https://doi.org/10.1063/5.0026220>

13 July 2025 19:34:33

I. INTRODUCTION

Whistler-mode waves are electromagnetic waves with a right-handed polarization,^{1–4} which are considered to play an important role in the Earth's radiation belt, including accelerating electrons to high energy and precipitating energetic electrons into the ionosphere.^{6–12} The magnetic equator can be one of the source regions of whistler-mode waves, where the dipole magnetic field reaches its minimum.^{3,4,13} It is commonly accepted that whistler-mode waves can be excited by an electron temperature anisotropy,^{3–5,14–18} whose dominant wave mode generally propagates along the background magnetic field (i.e., the wave normal angle $\theta \approx 0^\circ$).¹⁵ However, when the electron plasma beta is sufficiently small ($\beta_e \leq 0.025$), the propagation of the dominant wave mode tends to have a larger normal angle.^{19,20} One of the most typical properties of whistler-mode waves is the power gap around half the electron gyrofrequency, which can separate the waves into two frequency bands.^{21–25}

Satellite observations have shown that the whistler-mode waves are usually along with electron beams in the parallel velocity.^{23,26} Then, Sauer *et al.*²⁴ have suggested that these electrons can lead to the formation of a power gap in the whistler-mode waves. However, their results are only predicted by the linear theory. In this study, we want to extend their work by performing a parameter study to find that which is the key factor to determine the frequency of the power gap. Our results are supported by both linear theory analysis and particle-in-cell (PIC) simulations.

This paper is organized as follows. Section II describes the models and initial setup. The theoretical and simulation results are illustrated in Sec. III, and Sec. IV presents the principle conclusions and some discussions.

II. THEORETICAL AND PIC SIMULATION MODEL

In this paper, the plasma consists of three populations: cold electrons, hot electrons, and protons. The cold electrons are

TABLE I. The plasma parameters for cases 0–13.

Case	V_{D1}/V_{Ae}	V_{D2}/V_{Ae}	n_{bm}/n_h (%)	$\beta_{\parallel bm}$	$\beta_{\parallel bi}$	$T_{\perp bi}/T_{\parallel bi}$
0	0.00	...	0.09	4.0
1	0.6	0.6	1.80	0.0196	0.09	4.0
2	0.4	0.4	1.80	0.0196	0.09	4.0
3	0.8	0.8	1.80	0.0196	0.09	4.0
4	0.6	0.6	0.90	0.0196	0.09	4.0
5	0.6	0.6	3.60	0.0196	0.09	4.0
6	0.6	0.6	1.80	0.0100	0.09	4.0
7	0.6	0.6	1.80	0.0324	0.09	4.0
8	0.6	0.6	1.80	0.0196	0.05	4.0
9	0.6	0.6	1.80	0.0196	0.13	4.0
10	0.6	0.6	1.80	0.0196	0.09	3.0
11	0.6	0.6	1.80	0.0196	0.09	5.0
12	0.6	0.0	1.80	0.0196	0.09	4.0
13	0.6	0.8	1.80	0.0196	0.09	4.0

isotropic, whose temperature (T_c) is the same as that of protons, while hot electrons have a temperature anisotropy with beam-like shapes in the parallel velocity distribution. The number densities of cold and hot electrons are n_c and n_h , respectively, which satisfy $n_c + n_h = n_0$ (where n_0 is the total electron number density). In our study, the number density of hot electrons is fixed at $n_h/n_0 = 15\%$ ²⁷

and the plasma beta of cold electrons is $\beta_c = 2\mu_0 n_0 k_B T_c / B_0^2 = 10^{-4}$ (where μ_0 is the permeability of vacuum). The ratio of the plasma frequency to electron gyrofrequency is given as $\omega_{pe}/\Omega_e = 4.0$ ²⁸ (where $\omega_{pe} = \sqrt{n_0 e^2 / m_e \epsilon_0}$ and $\Omega_e = eB_0 / m_e$), and the light speed is $c = 4V_{Ae}$ (where $V_{Ae} = B_0 / \sqrt{\mu_0 n_0 m_e}$ is the electron Alfvén speed). The velocity distribution of hot electrons satisfies the following function:

$$f_h = n_{bi} (2\pi T_{\parallel bi} / m_e)^{-3/2} (T_{\perp bi} / T_{\parallel bi})^{-1} \\ \times \exp(-m_e v_{\parallel}^2 / 2T_{\parallel bi} - m_e v_{\perp}^2 / 2T_{\perp bi}) \\ + n_{bm} (2\pi T_{\parallel bm} / m_e)^{-3/2} (T_{\perp bi} / T_{\parallel bm})^{-1} \\ \times \exp(-m_e v_{\perp}^2 / 2T_{\perp bi} - m_e (v_{\parallel} - V_{D1})^2 / 2T_{\parallel bm}) \\ + n_{bm} (2\pi T_{\parallel bm} / m_e)^{-3/2} (T_{\perp bi} / T_{\parallel bm})^{-1} \\ \times \exp(-m_e v_{\perp}^2 / 2T_{\perp bi} - m_e (v_{\parallel} + V_{D2})^2 / 2T_{\parallel bm}), \quad (1)$$

where v_{\parallel} and v_{\perp} are the velocities parallel and perpendicular to the background magnetic field. The hot electrons can be considered to have three components: a bi-Maxwellian component (with the subscript “bi”), with the number density of n_{bi} and temperature anisotropy of $T_{\perp bi}/T_{\parallel bi}$, and two beam-like components (with the subscript “bm”), which have the same number density n_{bm} and

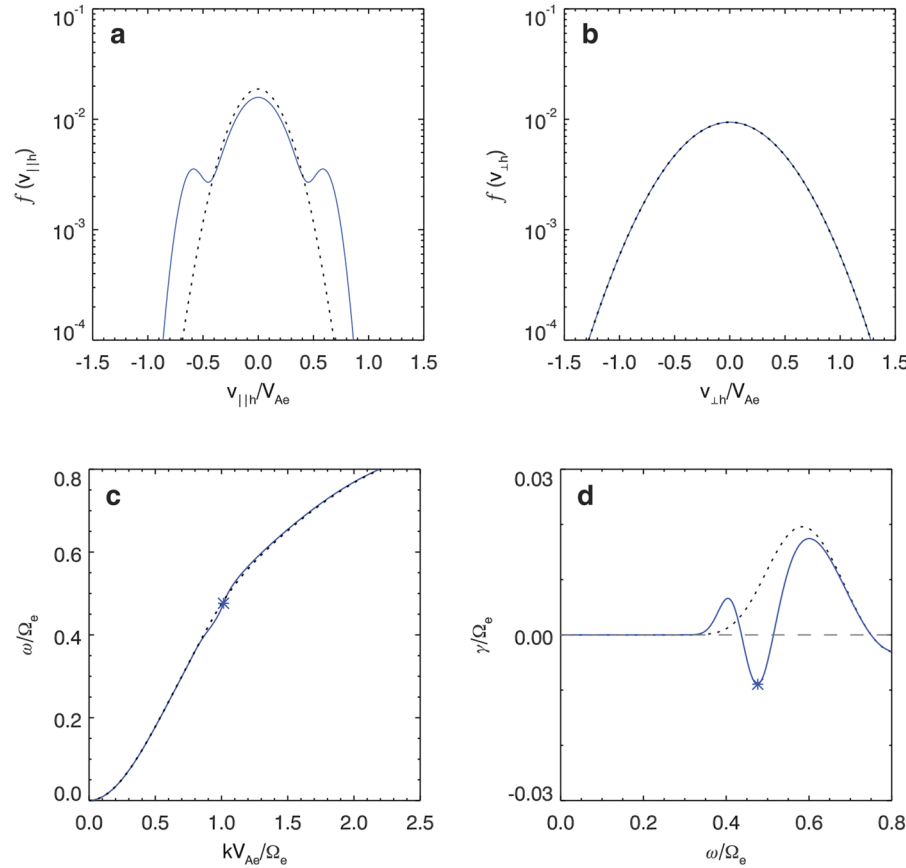


FIG. 1. The normalized velocity distributions in the (a) parallel and (b) perpendicular directions of the hot electrons, and (c) dispersion relations and (d) linear growth rates of whistler-mode waves in case 1 and case 0, which are denoted by blue solid and black dotted lines, respectively. The blue asterisks in (c) and (d) mark the frequency and wave number of the wave mode with the minimum growth rate between two growth peaks, and the gray dashed line in (d) denotes $\gamma = 0$.

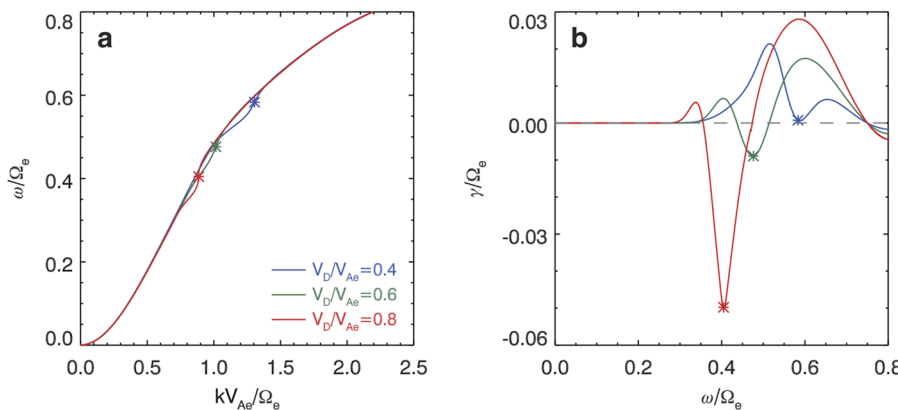


FIG. 2. The (a) dispersion relations and (b) growth rates of case 1 ($V_D = 0.6V_{Ae}$), case 2 ($V_D = 0.4V_{Ae}$), and case 3 ($V_D = 0.8V_{Ae}$), which are denoted by green, blue, and red lines, respectively. The wave modes with the minimum growth rate between two peaks are also marked by the asterisks in each colors.

satisfy $n_{bi} + 2n_{bm} = n_h$. V_{D1} and V_{D2} are the positions of beam-like shapes in the parallel and anti-parallel directions. A linear theory model, named as the kinetic plasma dispersion relation solver (PDRK),²⁹ has been employed to calculate the dispersion relation and linear growth rate. Here, we only show the wave modes with wave vectors along the background magnetic field since the waves always have the largest growth rate in the parallel direction in our cases (i.e., $\theta = 0^\circ$). Other wave normal angles have also been checked, while our main conclusions remain unchanged.

A 1D PIC simulation model with periodic boundary conditions has been employed to investigate the excitation of whistler-mode waves, which allows spatial variations only in the x direction. The protons are motionless (i.e., the mass ratio between the proton and electron is infinite) since the ion cyclotron frequency is much lower than the frequency of whistler-mode waves.^{17,18} The background magnetic field is along the x axis. The number of grid cells is 2048 with the grid size of $\Delta x = 0.20V_{Ae}/\Omega_e$, and the total simulation time is $1500\Omega_e^{-1}$ with the time step as $\Delta t = 0.025\Omega_e^{-1}$.

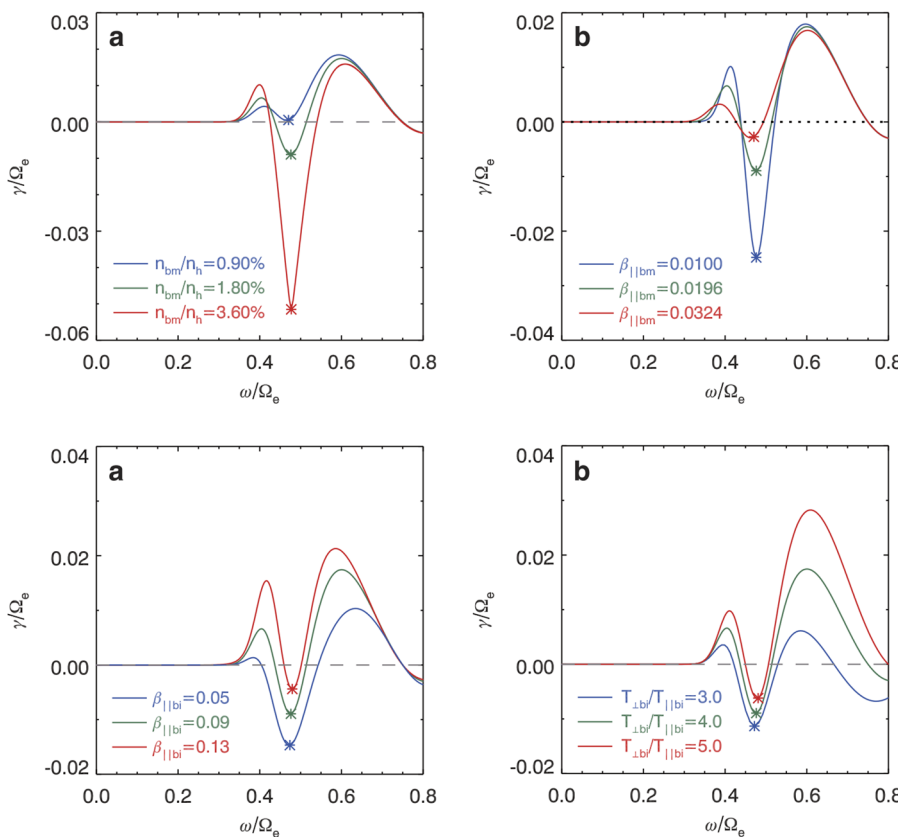


FIG. 3. The growth rates of whistler-mode waves in (a) case 1 ($n_{bm}/n_h = 1.8\%$, green line), case 4 ($n_{bm}/n_h = 0.9\%$, blue line), and case 5 ($n_{bm}/n_h = 3.6\%$, red line) and (b) case 1 ($\beta_{||bm} = 0.0196$, green line), case 6 ($\beta_{||bm} = 0.01$, blue line), and case 7 ($\beta_{||bm} = 0.0324$, red line).

FIG. 4. The growth rates of whistler-mode waves in (a) case 1 ($\beta_{||bi} = 0.09$, green line), case 8 ($\beta_{||bi} = 0.05$, blue line), and case 9 ($\beta_{||bi} = 0.13$, red line) and (b) case 1 ($T_{\perp bi}/T_{||bi} = 4.0$, green line), case 10 ($T_{\perp bi}/T_{||bi} = 3.0$, blue line), and case 11 ($T_{\perp bi}/T_{||bi} = 5.0$, red line).

We uniformly set an average of 6000 macroparticles per cell per species.

III. THEORETICAL AND SIMULATION RESULTS

In this paper, we will show the spectra of whistler-mode waves excited by an electron bi-Maxwellian distribution plus parallel beams. The influences of V_{D1} , V_{D2} , n_{bm}/n_h , $\beta_{\parallel bm}$ (the parallel plasma beta for the beam-like component, $\beta_{\parallel bm} = 2\mu_0 n_0 k_B T_{\parallel bm}/B_0^2$), $\beta_{\parallel bi}$ (the parallel plasma beta for the bi-Maxwellian component,

$\beta_{\parallel bi} = 2\mu_0 n_0 k_B T_{\parallel bi}/B_0^2$), and $T_{\perp bi}/T_{\parallel bi}$ are investigated. The detailed parameters for each case are listed in Table I.

In case 1, the position of the beam-like component is $V_{D1} = V_{D2} = V_D = 0.6V_{Ae}$, whose number density is $n_{bm}/n_h = 1.80\%$.²⁶ The parallel plasma betas of the beam-like component and the bi-Maxwellian component are $\beta_{\parallel bm} = 0.0196$ and $\beta_{\parallel bi} = 0.09$, and the temperature anisotropy of the bi-Maxwellian component is $T_{\perp bi}/T_{\parallel bi} = 4.0$.²⁸ Figure 1 shows the normalized velocity distributions of the hot electrons in the (a) parallel and (b) perpendicular directions and the (c) dispersion relation ($\omega-k$) and (d) linear growth rate (γ) of case 1, which are denoted by blue solid lines. The gray

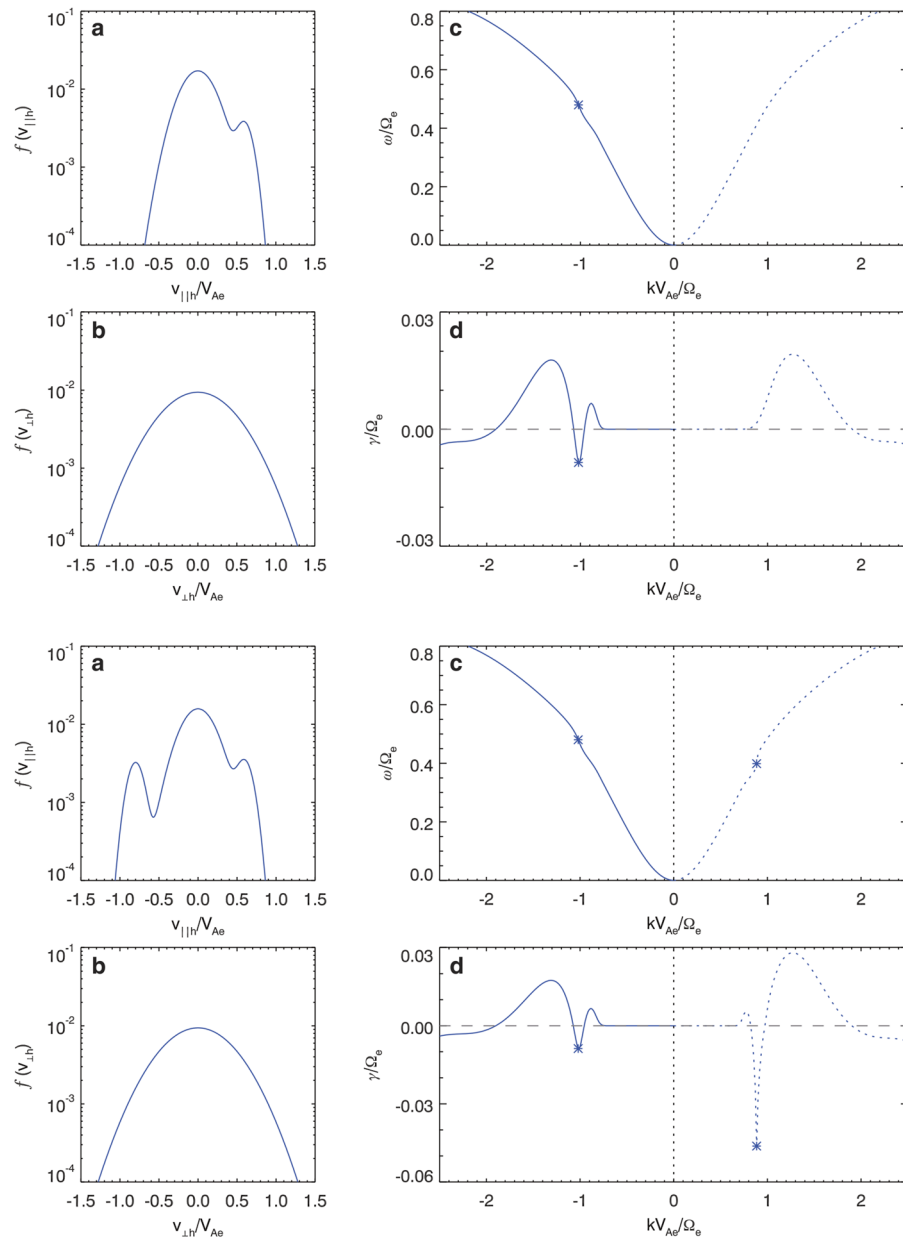


FIG. 5. The normalized velocity distributions of the hot electrons in (a) parallel and (b) perpendicular directions of case 12. (c) and (d) display the dispersion relation and growth rate of the whistler mode waves parallelly propagating (dotted lines) and anti-parallelly propagating (solid lines) along the background magnetic field. The asterisks mark the wave mode with the minimum growth rate between two growth peaks.

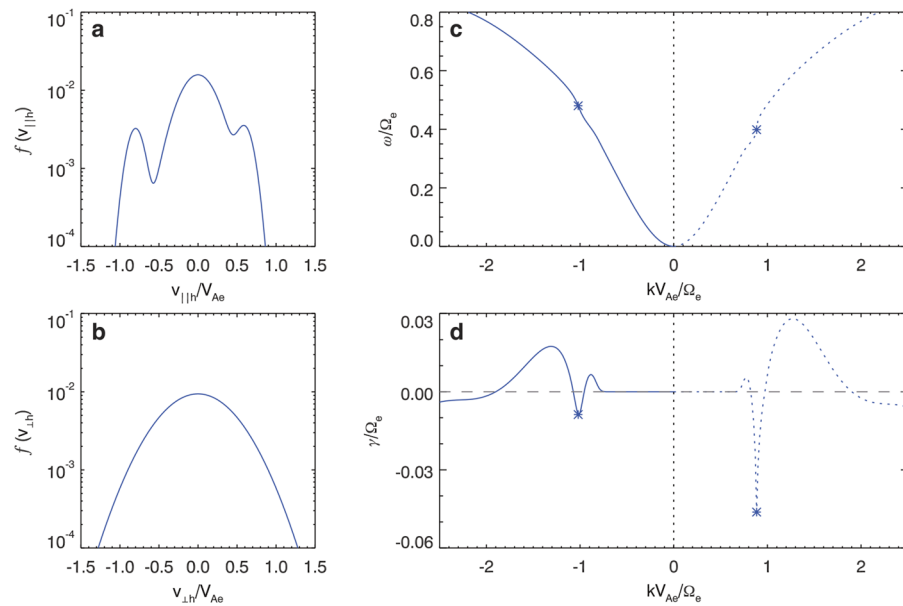


FIG. 6. The same format as Fig. 5, but for case 13, including the velocity distribution in (a) parallel and (b) perpendicular directions and the (c) dispersion relation and (d) growth rate of whistler-mode waves.

dashed line in Fig. 1(d) denotes $\gamma = 0$. For reference, we also plot a bi-Maxwellian velocity distribution with $T_{\perp bi}/T_{\parallel bi} = 4.0$ (hereafter referred to as case 0) and the corresponding dispersion relation and growth rate in this figure, represented by black dotted lines. The two dispersion relations are almost the same [Fig. 1(c)], except that the blue line has been a little bit distorted near $\omega/\Omega_e = 0.48$. When it comes to the growth rate in Fig. 1(d), the dominant wave mode in case 0 has the frequency as $\omega/\Omega_e = 0.58$ (with the wave number of $kV_{Ae}/\Omega_e = 1.28$). Meanwhile, the growth rate of the waves in case 1 has two peaks at about $\omega/\Omega_e = 0.41$ (with $kV_{Ae}/\Omega_e = 0.88$) and at about $\omega/\Omega_e = 0.41$ (with $kV_{Ae}/\Omega_e = 1.31$), leaving a clear gap around the frequency of $\omega/\Omega_e = 0.48$ (with $kV_{Ae}/\Omega_e = 1.01$, marked by the blue asterisks). In the gap, the growth rate is negative, indicating that the wave modes cannot be excited here.

Cases 2 and 3 illustrate the influences of the position of beam-like shapes on the wave spectra. Compared with case 1, in case 2,

$V_{D1} = V_{D2} = V_D = 0.4V_{Ae}$, and in case 3, $V_{D1} = V_{D2} = V_D = 0.8V_{Ae}$, while the other parameters are kept the same. Figure 2 shows the (a) dispersion relations and (b) growth rates of the whistler-mode waves in cases 1–3. The variation of V_D almost does not change the dispersion relation, except a little bit distorted. Unless otherwise stated, we will not show the dispersion relations hereafter since they remain almost unchanged for most of cases. However, the positions of the frequency gap are quite different. In cases 1, 2, and 3, the frequency gaps between two growth peaks are about $\omega/\Omega_e = 0.48$, $\omega/\Omega_e = 0.58$, and $\omega/\Omega_e = 0.41$, which are denoted by blue, green, and red asterisks, respectively. It is interesting to find that the position of the frequency gap increases with the decrease in V_D .

Compared with case 1, cases 4 and 5 change the values of n_{bm}/n_h . Figure 3(a) shows the growth rate for case 4 ($n_{bm}/n_h = 0.90\%$), case 1 ($n_{bm}/n_h = 1.80\%$), and case 5 ($n_{bm}/n_h = 3.60\%$). The variation of n_{bm}/n_h has little influence on the position of the gap

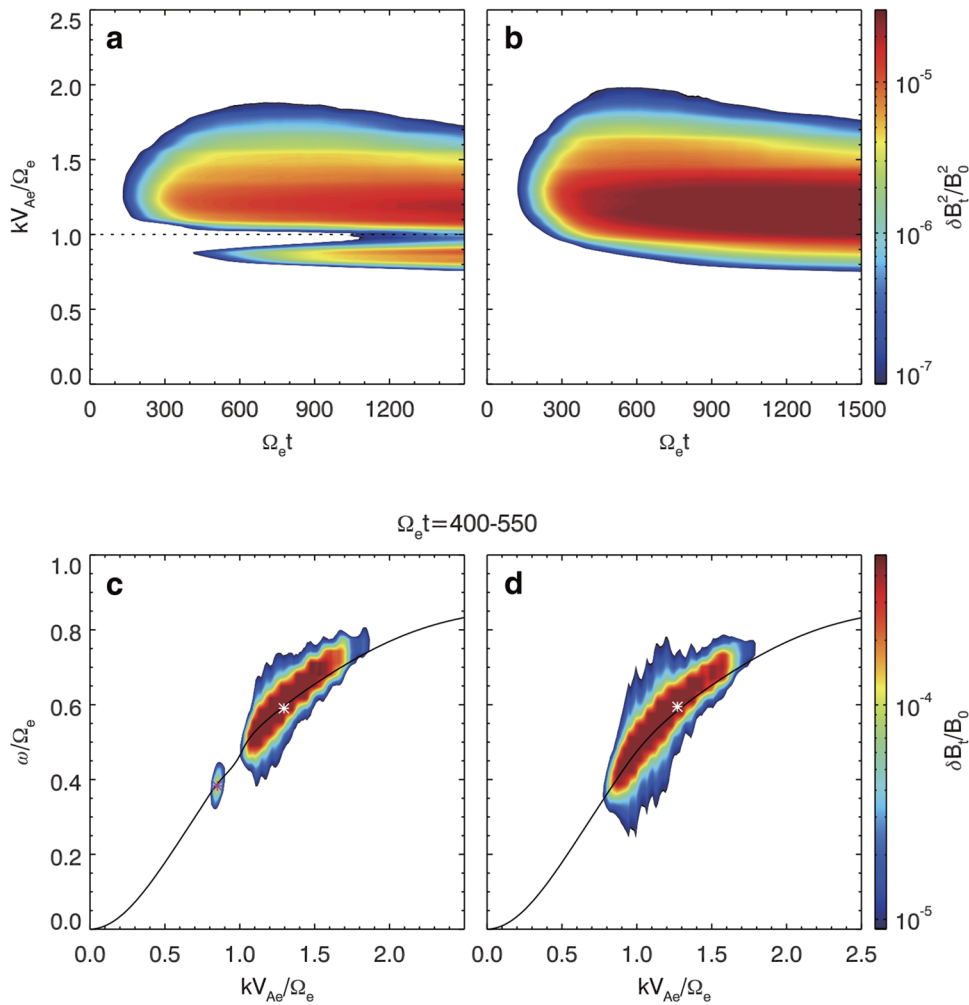


FIG. 7. The temporal evolution for the spectra of $\delta B_t^2/B_0^2$ in (a) case 1 and (b) case 0. The dotted line in (a) represents the wave number $kV_{Ae}/\Omega_e = 1.01$. The dispersion relations of the spectrograms in (c) case 1 and (d) case 0 during $\Omega_e t = 400-550$, where the black lines represent the dispersion relation curves from the linear theory analysis. In (c), the dominant wave modes in the two bands are denoted by the white and magenta stars. Meanwhile, the dominant mode in case 0 (d) is marked by a white star.

($\omega/\Omega_e \sim 0.48$). However, it has a great influence on the linear growth rate. The growth rates for case 6 ($\beta_{\parallel bm} = 0.01$), case 1 ($\beta_{\parallel p} = 0.0196$), and case 7 ($\beta_{\parallel p} = 0.0324$) are illustrated in Fig. 3(b). The position of the gap still remains almost unchanged.

Figure 4(a) illustrates the effects of $\beta_{\parallel bi}$. Compared with case 1 ($\beta_{\parallel bi} = 0.09$), $\beta_{\parallel bi}$ decreases to 0.05 in case 8 and increases to 0.13 in case 9. There are still two positive peaks, and their growth rates get larger with the increase in $\beta_{\parallel bi}$. Nevertheless, the variation of $\beta_{\parallel bi}$ almost has no influence on the position of the gap. Cases 10 and 11 show the influences of $T_{\perp bi}/T_{\parallel bi}$. The growth rates for case 10 ($T_{\perp bi}/T_{\parallel bi} = 3.0$), case 1 ($T_{\perp bi}/T_{\parallel bi} = 4.0$), and case 11 ($T_{\perp bi}/T_{\parallel bi} = 5.0$) are illustrated in Fig. 4(b). Similarly, the position of the gap still remains almost unchanged.

The beam-like components in the parallel and anti-parallel directions are symmetric (i.e., $V_{D1} = V_{D2}$) in the former cases. We have further investigated the growth rate in the two directions when V_{D1} is different from V_{D2} . Figure 5 shows the [(a) and (b)] normalized velocity distribution of the hot electrons, (c) dispersion relation, and (d) growth rate for case 12, in which there is only one beam-like component ($V_{D1} = 0.6V_{Ae}$). In Figs. 5(c) and 5(d), the parallel propagating and anti-parallel propagating waves are represented by dotted and solid lines, respectively. The existence of the beam-like shape in the parallel direction will lead to a frequency gap ($\omega/\Omega_e = 0.48$ and $kV_{Ae}/\Omega_e = -1.02$, represented by the blue asterisks) for the corresponding wave modes in the anti-parallel direction. Figure 6 is plotted in the same format with that of Fig. 5, but for case 13, which contains two asymmetric beam-like components ($V_{D1} = 0.6V_{Ae}$, while $V_{D2} = 0.8V_{Ae}$). As illustrated in Figs. 6(c) and 6(d), the gap in the parallel direction is caused by the beam-like component in the anti-parallel direction, and vice versa. The frequency gap for the corresponding wave modes in the parallel direction (with $\omega/\Omega_e = 0.41$ and $kV_{Ae}/\Omega_e = 0.89$) is different from that in the anti-parallel direction (with $\omega/\Omega_e = 0.48$ and $kV_{Ae}/\Omega_e = -1.02$). Therefore, the beam-like shape in one direction will lead to the formation of frequency gap in the opposite direction.

Even though theoretical analysis has shown the influences of the beam-like component, PIC simulations are still necessary to support these predictions. The temporal evolution for the spectra of whistler-mode waves in case 1 and case 0 has been investigated first. Figure 7 shows the $k-t$ spectrograms of the transverse fluctuating magnetic fields $\delta B_t^2/B_0^2$ ($\delta B_t^2 = \delta B_y^2 + \delta B_z^2$) in (a) case 1 and (b) case 0. The dotted line in Fig. 7(a) denotes the wave number $kV_{Ae}/\Omega_e = 1.01$ at the predicted frequency gap $\omega/\Omega_e = 0.48$. Obviously, there is a clear power gap around $kV_{Ae}/\Omega_e = 1.01$ in Fig. 7(a), which can divide the spectrum into two bands and still exist until the end of the simulation. Meanwhile, the spectrum in Fig. 7(b) has only one continuous band. The dispersion relations of the spectra in (c) case 1 and (d) case 0 in the time range $\Omega_e t = 400-550$ have also been shown in Fig. 7, where the black lines in each panel represent the dispersion relation curves from the linear theory prediction [Fig. 1(c)]. In case 1, the dominant wave modes with the maximum magnetic power in the two bands are located at $[1.29(V_{Ae}/\Omega_e)^{-1}, 0.59 \Omega_e]$ and $[0.85(V_{Ae}/\Omega_e)^{-1}, 0.38 \Omega_e]$, which have been marked by the white and magenta stars in Fig. 7(c), respectively. The white star in Fig. 7(d) denotes the dominant wave mode in case 0, with $kV_{Ae}/\Omega_e = 1.27$ and $\omega/\Omega_e = 0.59$. In Figs. 7(c) and 7(d), the dominant wave modes are close to the dispersion relation curves predicted from linear theory.

We have further investigated the influence of the position of beam-like shapes on the wave spectra. Figure 8 shows the temporal evolution of the wave spectra in (a) case 2 and (b) case 3. The dotted line in Fig. 8(a) represents the wave number $kV_{Ae}/\Omega_e = 1.30$ at the predicted frequency gap $\omega/\Omega_e = 0.58$, while that in Fig. 8(b) denotes $kV_{Ae}/\Omega_e = 0.89$ at $\omega/\Omega_e = 0.40$. There are two bands of waves in both cases, leaving a clear power minimum around $kV_{Ae}/\Omega_e = 1.30$ and $kV_{Ae}/\Omega_e = 0.89$, respectively. The position of the gap increases with the decrease in the position of beam-like shapes, which is consistent with the linear theory analysis (Fig. 2).

We have then performed another simulation case to investigate the influence of asymmetric beam-like components. Figure 9

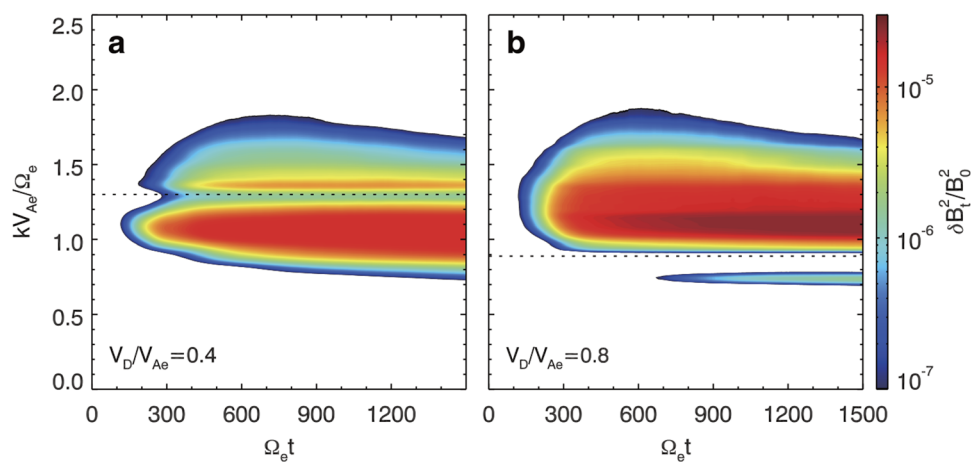


FIG. 8. The $k-t$ spectrograms of $\delta B_t^2/B_0^2$ in (a) case 2 (with $V_D/V_{Ae} = 0.4$) and (b) case 3 (with $V_D/V_{Ae} = 0.8$), where the dotted lines denote $kV_{Ae}/\Omega_e = 1.30$ and $kV_{Ae}/\Omega_e = 0.89$, respectively.

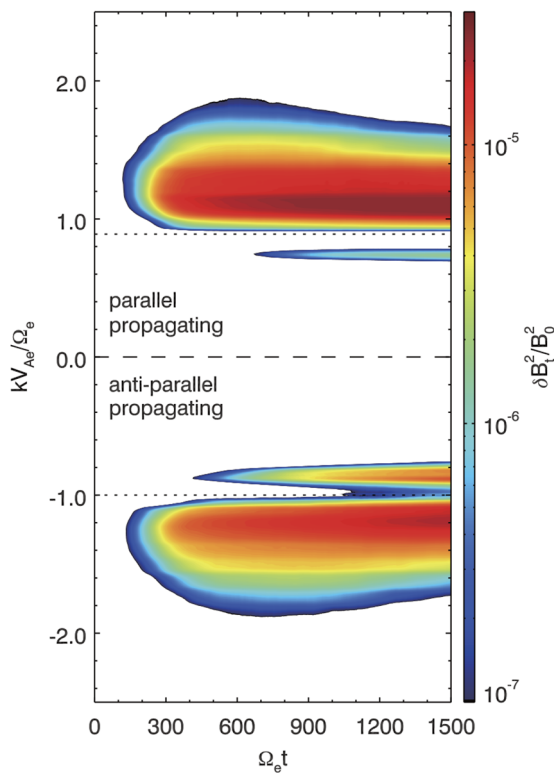


FIG. 9. The temporal evolution of the spectra in the $+x$ and $-x$ directions for case 13, where the black dotted lines denote the wave numbers of $kV_{Ae}/\Omega_e = 0.89$ and $kV_{Ae}/\Omega_e = -1.01$, respectively.

illustrates the temporal evolution of $\delta B_t^2/B_0^2$ in the $+x$ and $-x$ directions for case 13. The dotted lines denote $kV_{Ae}/\Omega_e = 0.89$ and $kV_{Ae}/\Omega_e = -1.01$, respectively. In the parallel direction, the power gap is around $kV_{Ae}/\Omega_e = 0.89$, while another power gap is around $kV_{Ae}/\Omega_e = -1.01$ in the anti-parallel direction. This result can verify the linear theory analysis, which has predicted that the beam-like component in one direction can lead to the formation of frequency gap in the spectra of waves propagating in the opposite direction.

IV. CONCLUSIONS AND DISCUSSION

In this paper, we have investigated the whistler-mode waves excited by an electron bi-Maxwellian distribution plus parallel beams. The growth rate has two positive peaks, but is negative around the gap, indicating that the waves should exhibit a two-band spectrum. We have further performed a parameter analysis to investigate the influences of different parameters on the wave spectra and found that the position of beam-like shape (V_D) can play the most important role in determining the frequency of power gap, which will decrease as V_D increases. Moreover, the beam-like shape on one direction can lead to the formation of frequency gap in the waves propagating in the opposite direction. Our results are supported by both theoretical analysis and PIC simulations.

Previous literature studies have indicated that the Landau damping can lead to the formation of a two-band spectrum in the

whistler-mode waves.^{30–32} Specifically, Omura *et al.*³¹ have suggested that the waves will experience strong nonlinear damping via Landau resonance around $0.5\Omega_e$, as they propagate to higher latitudes. Then, a test particle simulation has been performed to support this theory.³² However, in our study, the waves are parallel propagating and there is no parallel electric fields. Therefore, the Landau damping will not take effect. The power gap in the wave spectra is caused by the mode splitting of beam-like electrons, which can create a forbidden area in the $\omega-k$ plane³³ after the beam electrons are included in the system. These beam-like distributions are usually observed along with whistler-mode waves in the Earth's magnetosphere.^{23,26} However, their generation mechanism is still an open question and is left to further investigation. Our study can provide a comprehensive understanding of the effects of beam-like electrons on the spectrum of whistler-mode waves.

ACKNOWLEDGMENTS

This work was supported by the Strategic Priority Research Program of the Chinese Academy of Sciences (Grant No. XDB 41000000), the NSFC (Grant Nos. 41527804 and 41774151), the Young Elite Scientists Sponsorship Program by CAST (Grant No. 2018QNRC001), and the Key Research Program of Frontier Sciences, CAS (Grant No. QYZDJ-SSW-DQC010).

DATA AVAILABILITY

The data that support the findings of this study are openly available in NSSDC Space Science Article Data Repository at <https://dx.doi.org/10.12176/01.99.00158>, Ref. 34.

REFERENCES

- ¹C. F. Kennel and H. E. Petschek, “Limit on stably trapped particle fluxes,” *J. Geophys. Res.* **71**(1), 1–28, <https://doi.org/10.1029/JZ071i001p00001> (1966).
- ²W. J. Burtis and R. A. Helliwell, “Banded chorus—A new type of VLF radiation observed in the magnetosphere by OGO 1 and OGO 3,” *J. Geophys. Res.* **74**(11), 3002–3010, <https://doi.org/10.1029/JA074i011p03002> (1969).
- ³B. T. Tsurutani and E. J. Smith, “Postmidnight chorus: A substorm phenomenon,” *J. Geophys. Res.* **79**(1), 118–127, <https://doi.org/10.1029/JA079i001p00118> (1974).
- ⁴B. T. Tsurutani and E. J. Smith, “Two types of magnetospheric ELF chorus and their substorm dependences,” *J. Geophys. Res.* **82**(32), 5112–5128, <https://doi.org/10.1029/JA082i032p05112> (1977).
- ⁵Z. Li, Q. M. Lu, R. S. Wang, X. L. Gao, and H. Y. Chen, “*In situ* evidence of resonant interactions between energetic electrons and whistler waves in magnetopause reconnection,” *Earth Planet. Phys.* **3**(6), 1–473 (2019).
- ⁶D. Summers, R. M. Thorne, and F. Xiao, “Relativistic theory of wave-particle resonant diffusion with application to electron acceleration in the magnetosphere,” *J. Geophys. Res.* **103**(A9), 20487–20500, <https://doi.org/10.1029/98JA01740> (1998).
- ⁷R. B. Horne, R. M. Thorne, S. A. Glauert, J. M. Albert, N. P. Meredith, and R. R. Anderson, “Timescale for radiation belt electron acceleration by whistler mode chorus waves,” *J. Geophys. Res.* **110**, A03225, <https://doi.org/10.1029/2004JA010811> (2005).
- ⁸F. Xiao, Z. Su, H. Zheng, and S. Wang, “Modeling of outer radiation belt electron by multidimensional diffusion process,” *J. Geophys. Res.* **114**, A03201, <https://doi.org/10.1029/2008JA013580> (2009).
- ⁹R. M. Thorne, W. Li, B. Ni, Q. Ma, J. Bortnik, L. Chen, D. N. Baker, H. E. Spence, G. D. Reeves, M. G. Henderson *et al.*, “Rapid local acceleration of relativistic radiation-belt electrons by magnetospheric chorus,” *Nature* **504**(7480), 411 (2013).
- ¹⁰B. Ni, R. M. Thorne, Y. Y. Shprits, and J. Bortnik, “Resonant scattering of plasma sheet electrons by whistler-mode chorus: Contribution

- to diffuse auroral precipitation," *Geophys. Res. Lett.* **35**, L11106, <https://doi.org/10.1029/2008GL034032> (2008).
- ¹¹R. M. Thorne, B. Ni, X. Tao, R. B. Horne, and N. P. Meredith, "Scattering by chorus wave as the dominant cause of diffuse auroral precipitation," *Nature* **467**, 943–946 (2010).
- ¹²B. T. Tsurutani, G. S. Lakhina, and O. P. Verkhoglyadova, "Energetic electron (>10 keV) microburst precipitation, ~5–15 s X-ray pulsations, chorus, and wave-particle interactions: A review," *J. Geophys. Res.: Space Phys.* **118**, 2296–2312, <https://doi.org/10.1002/jgra.50264> (2013).
- ¹³C. T. Russel, R. E. Holzer, and E. J. Smith, "OGO 3 observations of ELF noise in the magnetosphere: 1. Spatial extent and frequency of occurrence," *J. Geophys. Res.* **74**(3), 755–777, <https://doi.org/10.1029/JA074i003p00755> (1969).
- ¹⁴P. J. Palmadesso and K. Papadopoulos, *Wave Instabilities in Space Plasmas* (Astrophysics and Space Science Library, 1979), p. 74.
- ¹⁵S. P. Gary and H. Karimabadi, "Linear theory of electron temperature anisotropy instabilities: Whistler, mirror, and Weibel," *J. Geophys. Res.* **111**, A11224, <https://doi.org/10.1029/2006JA011764> (2006).
- ¹⁶Q. M. Lu, L. Q. Wang, Y. Zhou, and S. Wang, "Electromagnetic instabilities excited by electron temperature anisotropy," *Chin. Phys. Lett.* **21**, 1518 (2004).
- ¹⁷Q. Lu, L. Zhou, and S. Wang, "Particle-in-cell simulations of whistler waves excited by an electron distribution in space plasma," *J. Geophys. Res.* **115**, A02213, <https://doi.org/10.1029/2009JA014580> (2010).
- ¹⁸H. Chen, X. Gao, Q. Lu, J. Sun, and S. Wang, "Nonlinear evolution of counter-propagating whistler mode waves excited by anisotropic electrons within the equatorial source region: 1-D PIC simulations," *J. Geophys. Res.: Space Phys.* **123**, 1200–1207, <https://doi.org/10.1002/2017JA024850> (2018).
- ¹⁹S. P. Gary, K. Liu, and D. Winske, "Whistler anisotropy instability at low electron: Particle-in-cell simulations," *Phys. Plasmas* **18**(8), 082902 (2011).
- ²⁰K. Fan, X. Gao, Q. Lu, J. Guo, and S. Wang, "The effects of thermal electrons on whistler mode waves excited by anisotropic hot electrons: Linear theory and 2-D PIC simulations," *J. Geophys. Res.: Space Phys.* **124**, 5234–5245, <https://doi.org/10.1029/2019ja026463> (2019).
- ²¹X. Gao, L. Chen, W. Li, Q. Lu, and S. Wang, "Statistical results of the power gap between lower-band and upper-band chorus waves," *Geophys. Res. Lett.* **46**, 4098–4105, <https://doi.org/10.1029/2019GL082140> (2019).
- ²²K. Liu, S. P. Gary, and D. Winske, "Excitation of banded whistler waves in the magnetosphere," *Geophys. Res. Lett.* **38**, L14108, <https://doi.org/10.1029/2011GL048375> (2011).
- ²³J. Li, J. Bortnik, X. An, W. Li, V. Angelopoulos, R. M. Thorne, C. T. Russell, B. Ni, X. Shen, W. S. Kurth *et al.*, "Origin of two-band chorus in the radiation belt of Earth," *Nat. Commun.* **10**, 4672 (2019).
- ²⁴K. Sauer, K. Baumgärtel, and R. Sydora, "Gap formation around $\Omega_e/2$ and generation of low-band whistler waves by Landau-resonant electrons in the magnetosphere: Predictions from dispersion theory," *Earth Planet. Phys.* **4**(2), 1–13 (2020).
- ²⁵H. Chen, X. Gao, Q. Lu, Y. Ke, and S. Wang, "Lower band cascade of whistler waves excited by anisotropic hot electrons: One-dimensional PIC simulations," *J. Geophys. Res.: Space Phys.* **122**, 10,448–10,457, <https://doi.org/10.1002/2017JA024513> (2017).
- ²⁶R. Chen, X. Gao, Q. Lu, and S. Wang, "Unraveling the correlation between chorus wave and electron beam-like distribution in the Earth's magnetosphere," *Geophys. Res. Lett.* **46**, 11671–11678, <https://doi.org/10.1029/2019GL085108> (2019).
- ²⁷X. Gao, W. Li, R. M. Thorne, J. Bortnik, V. Angelopoulos, Q. Lu, X. Tao, and S. Wang, "New evidence for generation mechanisms of discrete and hiss-like whistler mode waves," *Geophys. Res. Lett.* **41**, 4805–4811, <https://doi.org/10.1002/2014GL060707> (2014).
- ²⁸C. Yue, X. An, J. Bortnik, Q. Ma, W. Li, R. M. Thorne, G. D. Reeves, M. Gkioulidou, D. G. Mitchell, and C. A. Kletzing, "The relationship between the macroscopic state of electrons and the properties of chorus waves observed by the Van Allen probes," *Geophys. Res. Lett.* **43**, 7804–7812, <https://doi.org/10.1002/2016GL070084> (2016).
- ²⁹H. Xie and Y. Xiao, "PDRK: A general kinetic dispersion relation solver for magnetized plasma," *Plasma Sci. Technol.* **18**(2), 97–107 (2016).
- ³⁰F. V. Coroniti, F. L. Scarf, C. F. Kennel, and W. S. Kurth, "Analysis of chorus emissions at Jupiter," *J. Geophys. Res.* **89**, 3801–3820, <https://doi.org/10.1029/JA089iA06p03801> (1984).
- ³¹Y. Omura, M. Hikishima, Y. Katoh, D. Summers, and S. Yagitani, "Nonlinear mechanisms of lower-band and upper-band VLF chorus emissions in the magnetosphere," *J. Geophys. Res.* **114**, A07217, <https://doi.org/10.1029/2009JA014206> (2009).
- ³²Y.-K. Hsieh and Y. Omura, "Nonlinear damping of oblique whistler mode waves via Landau resonance," *J. Geophys. Res.: Space Phys.* **123**, 7462–7472, <https://doi.org/10.1029/2018JA025848> (2018).
- ³³K. Hashimoto and H. Matsumoto, "Temperature anisotropy and beam type whistler instabilities," *Phys. Fluids* **19**, 1507 (1976).
- ³⁴H. Chen, "Two-band whistler-mode waves excited by an electron bi-maxwellian distribution plus parallel beams: 1D PIC data," *NSSDC Space Science Article Data Repository* (2020).